Available online at www.sciencedirect.com
SCIENCE DIRECT®
International Journal of Heat and Mass Transfer 48 (2005) 5166–5178
International Journal of HEAT and MASS TRANSFER
www.elsevier.com/locate/ijhmt

A three-dimensional conjugate model with realistic boundary conditions for flow and heat transfer in an industry scale hydrothermal autoclave

Hongmin Li [a], Edward A. Evans [b,*], G.-X. Wang [a]

[a] Department of Mechanical Engineering, The University of Akron, Akron, OH 44325, USA
[b] Department of Chemical Engineering, The University of Akron, Akron, OH 44325, USA

Received 2 December 2004; received in revised form 30 July 2005
Available online 11 October 2005

Abstract

This paper presents a conjugate heat transfer model for industry size hydrothermal autoclaves. The electric heating on the wall outside surfaces is represented by constant heat fluxes. The circumferential heat flux deviation is introduced for the asymmetric factors from the surroundings. The results indicate that the temperature at the solution/wall interface is far from uniform. Circumferential temperature deviation is large enough to establish an asymmetric flow. To accurately simulate flows in industry autoclaves, one needs to use the conjugate model. The growth environment in current industry autoclaves, however, can be improved by establishing a uniform temperature on the wall/solution interface.

Keywords: Conjugate model; Natural convection; Hydrothermal; Crystal growth

1. Introduction

As the requirements for small piezoelectric devices become stringent, the quality of the single crystal components must be improved [1]. Most of the piezoelectric single crystals are obtained using the hydrothermal growth technique, which takes place in an autoclave at high temperatures (around 400 °C) and high pressure (1000 bar) [2]. Current autoclaves for growing quartz single crystals are cylindrical containers with thick walls made from low carbon steel [2], as shown schematically in Fig. 1. An autoclave, filled with aqueous solution, is partitioned by a baffle with an opening between a lower dissolving chamber and an upper growing chamber [3]. Raw crystal pellets are packed in the dissolving chamber, while the seed crystal plates are hung in the growing chamber. Outside the metal wall, two electric strip heaters are wrapped around the autoclave to provide the required high temperature environments in the chambers. To reduce the heat loss, thick layers of insulation material are wrapped around the assembly. For growing single crystal quartz, which has a positive solubility-temperature coefficient, the main heater supplies heat into the lower chamber. The secondary heater is used to compensate the heat loss from the upper chamber but maintains a temperature that is lower than the temperature in the dissolving chamber. The two heaters are

* Corresponding author. Tel.: +1 330 972 8292; fax: +1 330 972 5856.
E-mail address: evanse@uakron.edu (E.A. Evans).

0017-9310/$ - see front matter © 2005 Elsevier Ltd. All rights reserved.
doi:10.1016/j.ijheatmasstransfer.2005.07.015

Nomenclature

B	body force
D	autoclave inside diameter
$\vec{g}$	gravity vector
h	thermodynamic enthalpy
H	total enthalpy
H_A	autoclave inside height
q	heat flux on the wall outside surface
Q_{total}	total heat supply rate on lower chamber wall
R, θ, Z	cylindrical coordinates
Ra_D	Rayleigh number based on D
T_0	reference temperature
$\vec{U}$	velocity vector

Greek symbols

β	thermal expansion coefficient
δ	Kronecker delta
δq	heat flux deviation
ρ_0	fluid density at the reference temperature
κ	turbulence kinetic energy
ω	turbulence dissipation rate
μ	total viscosity
μ_0	molecular viscosity
μ_T	turbulence viscosity

independently controlled so that a temperature difference between the two chambers, about 10 °C, can be maintained during the entire growth process. During growth, the dissolved quartz is transported from the dissolving chamber to the upper growing chamber by the natural convection flow induced by the temperature difference between the two chambers. Since the upper growing chamber has a lower temperature, dissolved quartz is then precipitated out from the solution and deposited on the seed crystal plates.

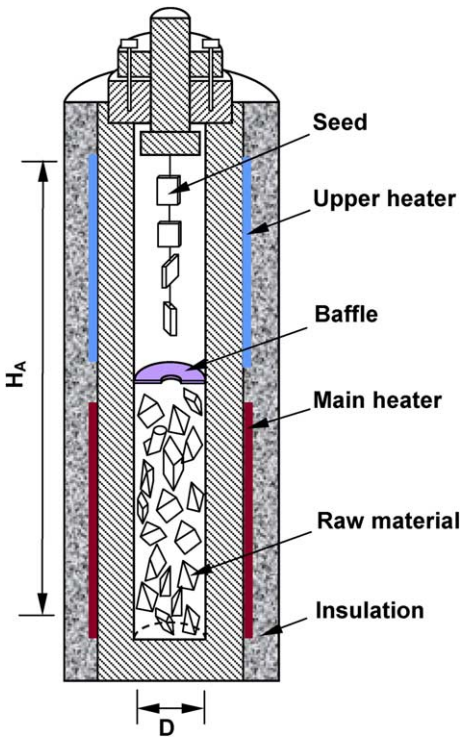

Fig. 1. A schematic of an industry autoclave for hydrothermal crystal growth. The aspect ratio is defined as H_A/D.

It has been shown that the flow of solution and the coupled temperature profile are critical to both the growth rate and growth quality [4,5]. The convection flow of solution is driven by the buoyancy force caused by the density variation in the fluid due to the concentration and temperature variations. Since the nutrient concentration variation is usually small, the convection is driven primarily by the temperature difference between the upper and lower chamber walls. Numerical models, including one conjugate model by Roux et al. [6] and several isothermal wall models [7–10], have been developed to investigate the flows in autoclaves. Roux's conjugate model, a model of steady laminar flow at low Rayleigh number, predicted a linear temperature distribution at the wall/solution interface from the bottom to the top. Roux's isothermal wall models, a two-dimensional (2-D) and a three-dimensional (3-D) one, are also for flow in the laminar regime, corresponding to autoclaves of very small size. Chen's isothermal wall model [7,8] considered unsteady laminar flow in an autoclave of low aspect ratio while focusing on the effects of the raw material region that was modeled as porous media. The 2-D isothermal wall model [9] and the 3-D one [10] by the present authors focused on the flow of solution in current industry size autoclaves with highly turbulent flows. The 2-D model in [9] assumed uniform temperature on the wall inner surface. The 3-D model in [10] questioned the isothermal wall assumption and superimposed a non-uniform temperature, called a temperature deviation, on the wall inner surface to represent the effects of the asymmetric factors resulting from the autoclave surroundings. The model predicted a one-cell asymmetric flow that agrees with what was found in industry growth practice and the speculated one by Kuznetsov and Lobachev [5].

As a summary, all the isothermal wall models were developed based on some kind of assumption on the

temperature of the wall inner surface. A circumferentially uniform temperature assumption resulted from the following speculation: A non-uniform temperature and heat flux established by the electrical heaters on the wall outer surface would be smeared out by the heat conduction in the thick metal wall. The temperature on the wall inner surface would be uniform. This so called isothermal wall assumption has no quantitative evidence to support its validity. Implementing a temperature deviation on the wall inner surface leads to a flow structure that agrees with the flow found in industry autoclaves [10]. Clearly, a determination of the temperature profile at the wall/solution interface is important.

In this paper, a 3-D conjugate model is developed. The fluid flow and heat transfer in an industry size autoclave are investigated with the model. In particular, the temperature and heat flux conditions on the wall inner surface (wall/solution interface) are examined in detail. For comparison, simulations are also conducted using the 2-D isothermal wall model and the 3-D model with temperature deviation to study the effect of the isothermal wall assumption and temperature deviation assumption. Finally, the flow and temperature fields, as growth environments, are analyzed and compared.

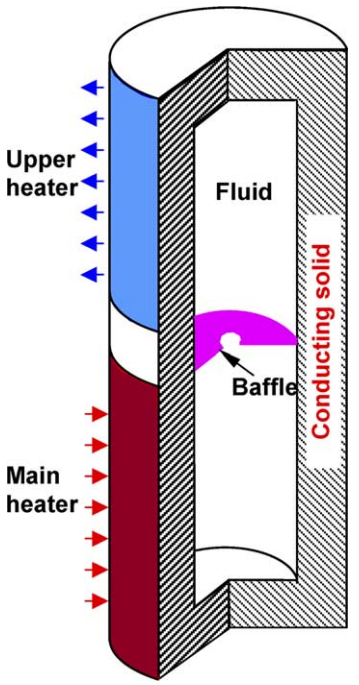

Fig. 2. Schematic of the conjugate model for the hydrothermal autoclave in Fig. 1.

2. Numerical model and mathematical formulation

2.1. Conjugate model

To study the flow and the heat transfer in the solution and heat conduction in the solid wall, a 3-D conjugate model is developed based on the following simplifications and assumptions: (1) the thickness of the sidewall, top wall, and bottom wall are assumed to be the same, (2) the effects of raw material and seed plates are not taken into account, (3) flows in industry autoclaves, with Rayleigh numbers based on autoclave diameter, Ra_D, in the order of 10^{12}, are expected to be highly turbulent [5,6], (4) heat conduction through the solid baffle is negligible and the thickness of the baffle can be neglected [9], (5) the heaters, usually thin electric resistors on the outside surface of the metal walls, and the insulation layers are used to maintain constant heat fluxes on the two walls. In the conjugate model, constant heat fluxes on the outside surfaces of the walls represent the overall effect of the heaters and the insulation layer. With the above simplifications and assumptions, fluid flow in an autoclave is simplified into the natural convection flow in a cylindrical container shown in Fig. 2.

Fig. 3 gives the computational domain and the thermal boundaries. The domain includes both the fluid and the metallic walls. Constant heat flux conditions are on the chamber wall outside surfaces to mimic the overall effects of electrical heaters and the insulation layer. The region between the heaters ($\Delta L = D$) is set to adiabatic since this region is usually used as a supporting structure. The top and bottom of the autoclave are assumed adiabatic because usually the autoclave is seated on a cement base and the top of the autoclave is well insulated.

Heat fluxes on the outside surface of the metallic wall are set circumferentially non-uniform. In other words a heat flux deviation, δq, is superimposed on the uniform heat flux on the metal wall outside surfaces. The total heat flow rate $Q_{\text{total}} = 3650$ W and the average heat flux $q = 1600$ W/m^2. Circumferentially non-uniform heating, or heat flux deviation, which is found in industry growth practice, is caused by the autoclave surroundings, non-uniform heater arrangements, and/or non-uniform insulation layers. As an example, considering the situation described in Fig. 3a, the heat supply into the metallic wall on the lower dissolving chamber at the right side is higher than average. Accordingly, the out going heat flow from the metallic wall of the upper growing chamber at the left side is higher than average. The heat flux boundaries are arranged to represent the heating conditions found in practice. On the dissolving chamber, the heat inflow rate is higher at the right side (from $\theta = 315°$ to $\theta = 45°$) and lower at the left side (from $\theta = 135°$ to $\theta = 225°$). The heat flow rate deviation is δq. The back and front regions have uniform average heat flux. For the upper growing chamber, heat outflow

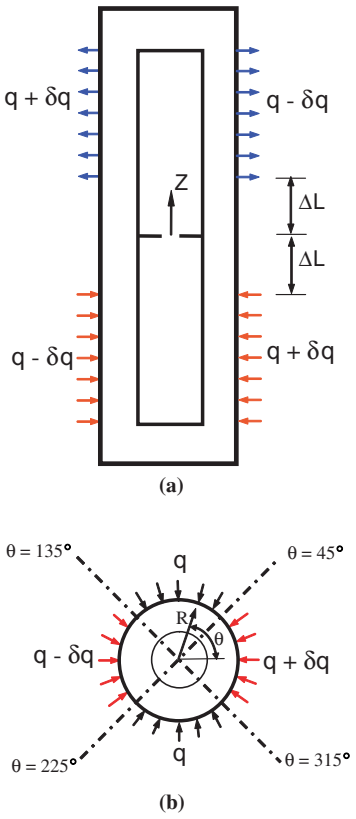

Fig. 3. Numerical domain and thermal boundary conditions of the three-dimensional conjugate model. (a) Side view and (b) top view of the lower chamber.

is higher at the left side and lower at the right side with the same deviation δq.

The ratio of δq over q is selected based on the current industry size autoclaves with their normal surrounding environments and experimental temperature data on the outside surface of the wall. Experimental data on industrial autoclaves only gives the total power supply to the heaters. There are no quantitative data on the wall heat flux and its variations on the outside surface of the metallic wall. However, temperature measurements on the outside surface of the metal wall show that temperature variation on the surface is around 2 °C. A simple calculation showed that a 2 °C temperature variation corresponds to a heat flux deviation of 10% of the average heat flux on the outside surface. Accordingly, the heat flux deviation over average heat flux, $\delta q/q$, is set to 10% in this study.

2.2. Mathematical formulation

The conjugate heat transfer and fluid flow model consists of the fluid domain for flow of solution and the solid domain for the metal wall. The governing equations in the fluid domain are the continuity equation, momentum equation (Navier–Stokes equation), the turbulence quantities determined by the turbulence κ–ω model [11], and the energy transport equation. In the solid domain, the governing equation is the heat conduction equation. These equations, in vector format, are given in Eqs. (1)–(9).

Continuity equation:

$$\nabla \cdot \left(\rho_0 \vec{U}\right) = 0 \tag{1}$$

Momentum equation:

$$\frac{\partial\left(\rho_0 \vec{U}\right)}{\partial t} + \nabla \cdot \left(\rho_0 \vec{U} \cdot \vec{U}\right) = \vec{B} - \nabla p + \mu \nabla^2 \vec{U} \tag{2}$$

$B = \rho \cdot \vec{g} \cdot \beta \cdot (T - T_0)$ is the body force where β is the thermal expansion coefficient.

Energy equation:

$$\frac{\partial \rho_0 H}{\partial t} + \nabla \cdot \left(\rho_0 \vec{U} H\right) - \nabla \cdot (k \nabla T) = \frac{\partial p}{\partial t} \tag{3}$$

where H is the total enthalpy including thermodynamic enthalpy and kinetic energy.

$$H = h + \frac{1}{2}\vec{U} \cdot \vec{U} \tag{4}$$

The fluid (aqueous solution) in the autoclave is treated as an incompressible fluid. Density is constant in the momentum equation except in the body force term (Boussinesq approximation):

$$\rho = \rho_0 \cdot [1 - \beta(T - T_0)] \tag{5}$$

T_0 is a reference temperature and is set to the average of T_H and T_L. ρ_0 is the density of the fluid at T_0.

Turbulent transport equations:

The viscosity in the momentum equation, Eq. (2), is the total viscosity including molecular viscosity, μ_0, and turbulence viscosity, μ_T:

$$\mu = \mu_0 + \mu_T \tag{6}$$

where the turbulence viscosity is calculated based on the relation: $\mu_T = \rho_0 \kappa/\omega$ with κ the turbulence kinetic energy and ω is the rate of dissipation of energy per unit volume. The Wilcox κ–ω turbulent transport equations are employed to determine κ and ω [12,13]:

$$\rho_0 \frac{\partial \kappa}{\partial t} + \rho_0 \vec{U} \cdot \nabla \kappa = \bar{\bar{\tau}} : \nabla \vec{U} - \beta^* \rho_0 \kappa \omega + \nabla \cdot [(\mu + \sigma^* \mu_T) \nabla \kappa] \tag{7}$$

$$\rho_0 \frac{\partial \omega}{\partial t} + \rho_0 \vec{U} \cdot \nabla \omega = \alpha^* \frac{\omega}{\kappa} \cdot \bar{\bar{\tau}} : \nabla \vec{U} - \beta^{**} \rho_0 \omega^2 + \nabla \cdot [(\mu + \sigma^{**} \mu_T) \nabla \omega] \tag{8}$$

$\bar{\bar{\tau}}$ is the stress tensor defined by $\bar{\bar{\tau}} = -p\delta + \mu(\nabla \vec{U} + \nabla \vec{U}^{\mathrm{T}})$.

The coefficients, given by the model developer and used in the Eqs. (7) and (8), are $\alpha^* = 5/9$, $\beta^* = 9/100$, $\beta^{**} = 3/40$, and $\sigma^* = \sigma^{**} = 1/2$ respectively [12].

Heat conduction in the metal wall:

Heat conduction in the metal wall is governed by the Laplace equation

$$\nabla^2 T = 0 \tag{9}$$

For the Navier–Stokes equations and turbulence equations, the boundary conditions, a non-slipping wall condition with turbulence kinetic energy (κ) equal to zero, are set on the wall inner surfaces. The boundary conditions for the heat conduction equation in the metal wall are set on the wall outside surfaces. On the wall inner surfaces, no thermal boundary condition is needed since the temperature is determined by the two energy equations, the energy transport equation in the fluid domain and the heat conduction equation in the wall.

2.3. Isothermal wall models

The purpose of the conjugate model developed in this paper is not only to investigate the realistic flow and temperature in current industry autoclaves, but also to validate or assess the previous modeling efforts with the isothermal wall models. A schematic of the 3-D isothermal wall model, developed in [10], is given in Fig. 4. The thermal boundary conditions on walls are two constant temperatures at T_H and T_L with superimposed temperature deviations. The two-dimensional isothermal model developed in [9] has the same geometry as shown in Fig. 4 while the thermal boundary conditions on walls are two constant temperatures without temperature deviation. In the 2-D model, both the geometry and the boundary conditions are axially symmetric. In order to make the modeling results of the conjugate model and the isothermal wall models qualitative and quantitatively comparable, the temperatures on the wall/solution interface obtained with the conjugate model are used as the boundary condition input to the isothermal wall models.

The primary difference between the conjugate model and the isothermal model is on the boundary conditions. In the conjugate model the boundary conditions are on the wall outside surface. The thermal condition on the wall/solution interface is determined during the simulation by the conduction in the metal wall and the convection in the fluid. In the isothermal wall model since only the flow in the fluid domain is simulated, the thermal conditions on the wall solution interface, which is the boundary of the fluid domain, must be given. In all previous investigations, the thermal conditions on the interface are assumed based on the isothermal wall assumptions discussed above.

The mathematical formulations of the isothermal models include all partial differential equations in the conjugate model other than the heat conduction equation for the metal wall. The equation sets of these models are solved by the same numerical scheme and the same under relaxation factors, and the grid independence has been checked.

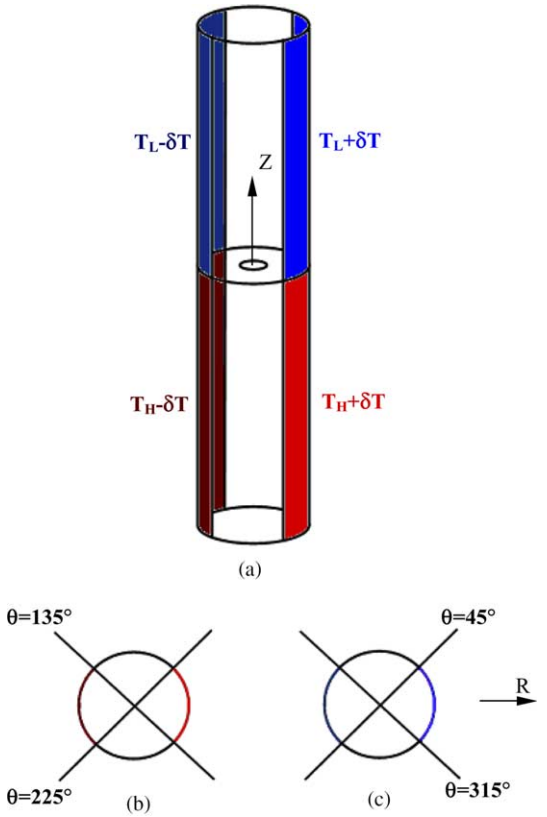

Fig. 4. Schematic of the three-dimensional isothermal wall model. (a) Geometry and boundaries, (b) cross-section of the lower chamber and (c) cross-section of the upper chamber.

2.4. Numerical solution

The above mathematical formulations, together with the boundary conditions described above, are solved with a commercial CFD software package called CFX, which uses the finite volume numerical scheme [11,12]. The under relaxation factors for continuity, momentum, and energy equations are 0.7, 0.7, 0.9 respectively. A structured non-uniform grid is used. To increase the confidence on the numerical simulation results, grid independence is checked for all the three models. For the conjugate model, flow is simulated with three sets of grids. The grid sizes and the corresponding predicted temperature at the center of the upper chamber ($R = 0$, $Z/D = 2.5$) are listed in Table 1. The differences between the results from the Grid #2 and Grid #3 are less than 0.7%. Results presented in this paper are obtained with the Grid #3. All the simulations are carried out on

Table 1
Grid independence study for the conjugate model

Grid	Grid size ($R\theta Z$)	$T - T_m$, °C	Difference $\lvert T_i - T_{i-1}\rvert / T_{i-1}$
Grid #1	$30 \times 32 \times 100$	$T_1 = -4.335$	
Grid #2	$60 \times 64 \times 200$	$T_2 = -4.205$	3.0%
Grid #3	$120 \times 128 \times 300$	$T_3 = -4.178$	0.64%

two SUN SPARC II workstations each has one Utra-SPARC II 400 MHz processor and one gigabyte memory.

3. Validation of the models

Due to the difficulties associated with the experiments under the high pressure and high temperature growth conditions, experimental data directly measured in industry autoclaves are not available in the literature to date. All the numerical models used in previous investigations are not directly validated.

Recently Ampofo and Karayiannis [13] experimentally measured the flow velocity and temperature in a rectangular enclosure with one sidewall heated and one sidewall cooled. The Rayleigh number based on the enclosure width is 1.58×10^9. The natural convection flow established in the enclosure is well in the fully turbulent regime. The experimental data will be used to validate the models developed in this paper. Since in Ampofo's experiments the hot wall and the cold wall are heated/cooled with controlled uniform temperature, there is no associated heat conduction. For the isothermal wall models, which consist of the continuity equation, momentum equations, energy equation, and the equations for turbulence quantities, the validation is complete. For the conjugate model, only simulation in the fluid domain has been validated.

The experimental test section used by Ampofo et al., as shown in Fig. 5a, is an enclosure of 750 mm in width, 750 mm in height, and 1500 mm in depth. One sidewall (ADD′A′) is at a uniform higher temperature, 50 °C, while the other sidewall (BCC′B′) is at a lower temperature, 10 °C. The temperatures on the top wall (DCC′D′) and the bottom wall (ABB′A′) are measured. The wall in the front and the back are well insulated. Temperature and vertical velocity in the enclosure are measured along the horizontal centerline, which is the line passing through the centers of the two sidewalls (ADD′A′ and BCC′B′).

The numerical model developed in this paper is used to simulate the flow and heat transfer in the above experimental rectangular enclosure. The numerical results are compared to the experimentally measured data. Fig. 5b shows the temperature and vertical velocity distribution along the horizontal centerline. One can see that the agreement is reasonably good. With the above experimental validation, the numerical models will be used to carry out the simulation of flow and heat transfer in industry autoclaves with more confidence.

4. Results and discussion

Fluid flow and heat transfer in an industry size autoclave are first simulated with the conjugate model. The flow profile and temperature field are obtained. Then the temperature and temperature deviation on the wall inner surface are used as boundary conditions for the two isothermal wall models. Flow and temperature profiles from the three models are compared to analyze the effects of the isothermal wall assumption.

4.1. Conjugate model simulation

4.1.1. Flow structure and temperature fields

Fig. 6a shows the flow structure in the symmetry ($\theta = 0°$) plane obtained using the 3-D conjugate model. The flow consists of two flow cells, one in each chamber and separated by the baffle. In both chambers, the flow cell is upward at the right side and downward at the left side. The one-cell flow direction agrees with the superimposed heat flux deviation on the wall outside surfaces, positive δq at the right side ($\theta = 0°$) and negative δq at the left side ($\theta = 180°$). The heat and fluid exchange between the two flow cells is through the baffle opening. For the flow cell in the upper chamber, the fluid temperature increases after passing by the baffle opening due to the heat transfer from and fluid exchange with the lower chamber. Higher temperature fluid from the lower chamber is mixed into the upper chamber flow cell. This higher temperature fluid rises up along the right side wall and turns at the top of the upper chamber. The downward going fluid at the left side continuously loses heat until it reaches the baffle where the flow makes another turn followed by the fluid exchange through the baffle opening. A similar flow process occurs in the lower chamber. The two flow cells, each occupies a chamber, are three-dimensional. The three-dimensional structure of the flow cells can be seen in Fig. 6b, which shows the vertical velocity (Z-velocity) magnitude on various horizontal cross-sections.

One can see that the upward flow and the down ward flow are asymmetric and occupy roughly the same amount of space with the upward flow at the right side and the downward flow at the left side in the upper chamber. The fluid near the vertical centerline (Z-axis) has relatively low velocity. Fig. 6c shows the temperature distribution in various cross-sections for both the fluid and the metallic wall. It can be seen that large temperature gradients exist in the metal wall. In the mean time temperature on the wall outside surface varies,

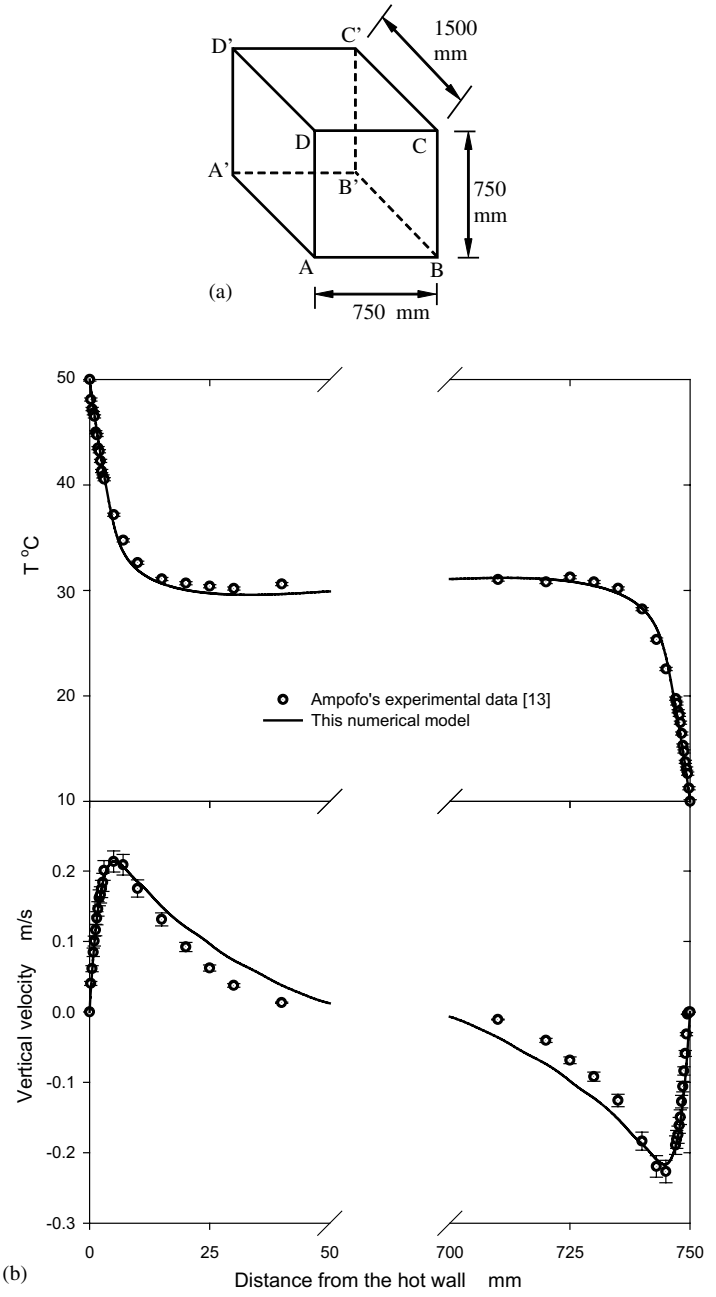

Fig. 5. Experimental validation of the numerical models. (a) A schematic of the experimental enclosure used by Ampofo et al. in [13] and (b) comparisons of the numerical and experimental temperature and vertical velocity distributions along the horizontal centerline.

which agrees with what was found in industry growth reality. It is noticeable that temperature also varies on the wall inner surface in both the vertical and circumferential directions. Quantitative data of temperature distribution on the wall inner surface is given later in this paper.

Temperature of the fluid in the lower chamber is higher than that of the fluid in the upper chamber. Temperature is not uniform in the horizontal direction due to the change of flow direction in the flow streams. In the upper chamber, the upward flow at the right side carries higher temperature fluid. Accordingly fluid at the left side has a lower temperature. In the lower chamber, the temperature of the downward flow is lower than that of the upward flow at the right side because of the low temperature fluid exchanged from the upper chamber.

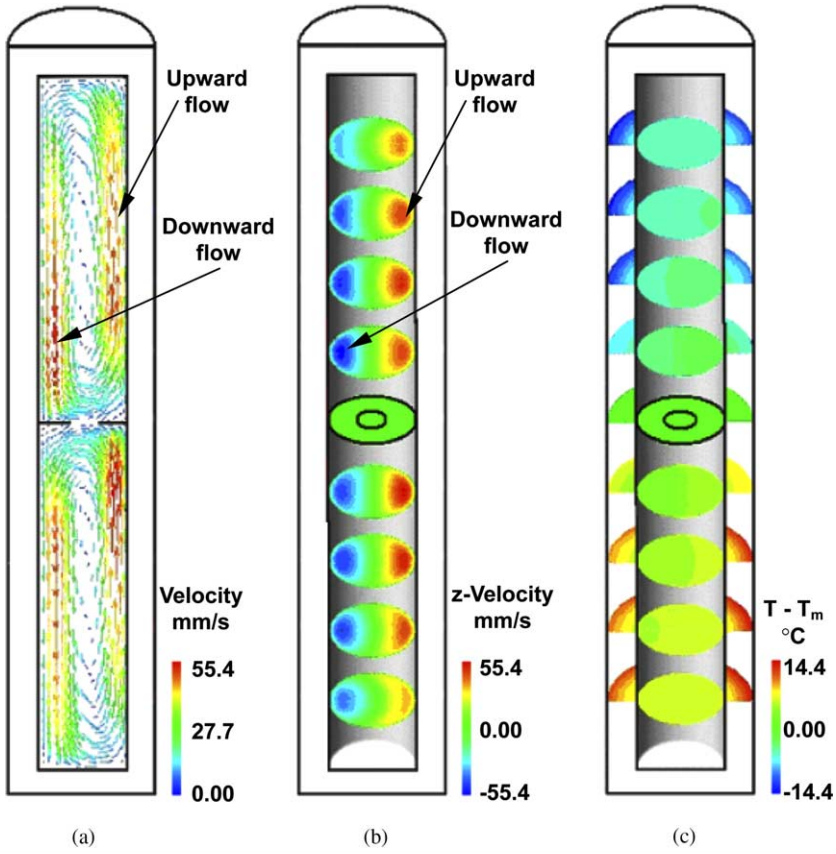

Fig. 6. Velocity and temperature profiles obtained with the conjugate model. (a) Velocity vector plot in the symmetry plane, (b) velocity magnitude in various horizontal cross-sections and (c) temperature distribution in various horizontal cross-sections.

The flow structure and temperature fields obtained in this paper using the conjugate model agree qualitatively with those speculated by Kuznetsov and Lobachev [5] and experimentally obtained by Klipov and Shmakov [4].

4.1.2. Temperature on the wall inner surface

The realistic temperature distribution on the wall inner surface is critical for isothermal wall models since in those models the wall inner surface is the boundary, on which thermal conditions have to be set and assumptions (such as the isothermal wall assumption) have to be made. We now examine the temperature distribution obtained with the conjugate model and then validate the assumptions and simplifications in the previous isothermal wall models.

In the cylindrical coordinate system shown in Fig. 3, the wall inner surface is a constant R plane. Fig. 7a shows the temperature variation on the wall inner surface in the vertical direction at three circumferential locations determined from the conjugate heat transfer model. One can see that temperature is not uniform on the wall inner surface in both chambers. The region around $\theta = 0°$ is at a higher temperature while a lower temperature is found in the region around $\theta = 180°$. Temperature variation on the interface is around 5 °C in the vertical direction from the baffle to the top of the upper chamber. The uniform wall temperature assumption in the isothermal wall models, as shown by the dashed line, is questionable. (Isothermal wall models assume constant temperature between Z/D equal to 1 and 5. In the section between Z/D equal to 0–1, various assumptions were made such as adiabatic wall in [8] and a sinusoidal distribution in [7].)

The horizontal temperature variation on the wall inner surface is shown in Fig. 7b. It can be seen that in the circumferential direction there is no temperature jump on the interface, which indicates that the heat flux jumps on the wall outside surface at $\theta = -45°$, 45°, 135°, 225° as shown in Fig. 3 caused by the superimposed heat flux deviation are smoothed out by heat conduction in the wall. The magnitude of the circumferential temperature variation is not the same for different height locations. At $Z/D = 1$, the variation from $\theta = 0°$ to $\theta = 180°$ is around 1.9 °C while at $Z/D = 4$ the corresponding variation is 0.8 °C. It is found by examining the temperature

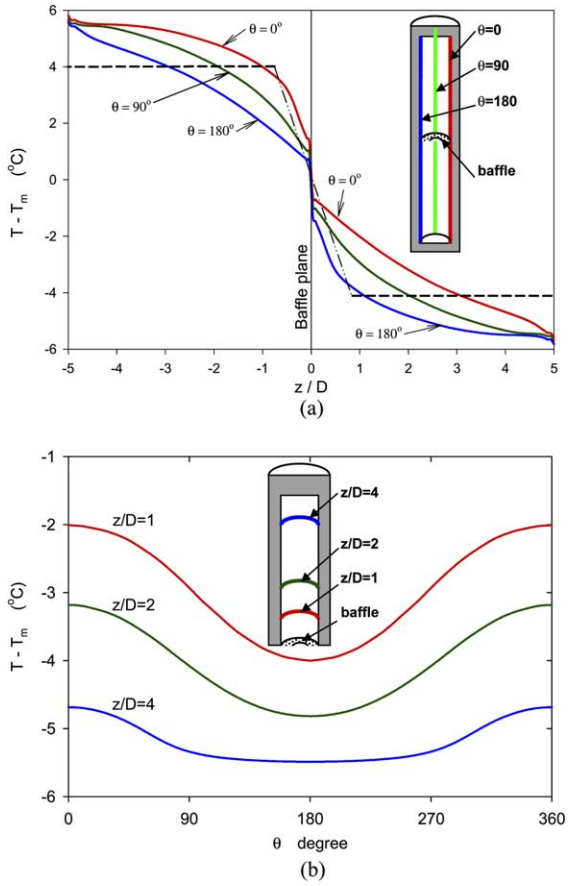

Fig. 7. Temperature variation on the wall/solution interface obtained with the conjugate model. (a) Vertical distribution at three circumferential locations and (b) horizontal distributions at three heights.

data on the wall inner surface that the temperature deviation reaches its maximum of 2.0 °C at $Z/D = 0.8$. The assumed vertically uniform temperature deviation in the three-dimensional model is also questionable. The assumed boundary temperature, uniformly distributed in both vertically and horizontally directions, in the 2-D isothermal wall model makes the model an ideal one.

4.1.3. Heat flux on the wall inner surface

Fig. 8 shows the nondimensionalized outgoing (in the positive R-direction) heat flux, on the wall inner surface in the upper chamber, along the vertical (Z) direction at three circumferential locations. q_0 is a nominal average heat flux calculated by the total heat flow rate on the upper chamber wall outside surface divided by the total area of the wall inner surface. With $Q_{\text{total}} = 3650$ W, the $q_0 = 2670$ W/m^2. It can be seen that the wall inner surface can be divided into four regions based on the heat

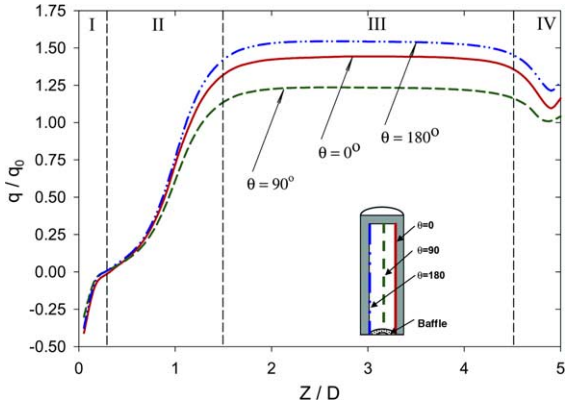

Fig. 8. Heat flux on the wall/solution interface in the upper chamber at three circumferential locations, obtained with the conjugate model.

flux distribution. Region I is very close to the baffle, from the baffle to $Z/D = 0.3$. Different from other part of the upper chamber wall, heat flow is from the wall into the solution due to the heat conduction in the wall from the lower chamber. Other than Region I, heat flow is from the solution into the solid wall. Region II is a transition region from $Z/D = 0.3$ to $Z/D = 1.5$. In this region the heat flux changes rapidly in the vertical direction. It should be noted that the uniform heat flux boundary, on the outside surface of the upper chamber wall, is from $Z/D = 1$ to $Z/D = 5$. Region III is the constant heat flux region, where heat flux variation in the vertical direction is small. Region IV is at the top of the upper chamber from $Z/D = 4.5$ to the top of the upper chamber. Because of the heat conduction in the top wall, the turning around of the flow at the top, and the flow stagnation at the corner, heat flux in Region IV is lower than in Region III.

In the circumferential direction, heat flux is noticeably higher at $\theta = 0°$ and $\theta = 180°$ than at $\theta = 90°$ because the upward stream (at $\theta = 0°$) and the downward stream (at $\theta = 180°$) cause strong convection on the wall. Comparatively at $\theta = 90°$ between the upward and downward stream, the flow velocity is lower than in the streams and the heat convection on the wall solution surface is weaker (see also Fig. 6). The difference between heat flux at $\theta = 0°$ and at $\theta = 180°$ is established by asymmetric factors, represented by the heat flux deviation imposed on the wall outside surface in this model.

From the temperature distribution at the wall–solution interface obtained by the conjugate model, we can estimate the averages temperature in the upper chamber $T - T_{\text{m}} = 4$ °C and the temperature deviation $\delta T = 0.3$ °C where T_{m} is the volume average temperature in the fluid domain. With these temperatures data as boundary conditions for the isothermal wall models (see Refs. [6–9] for detailed description), two

simulations, one with the 3-D isothermal wall model and one with the 2-D isothermal wall model, are carried out.

4.2. Isothermal wall model simulations

With the average temperature and the average temperature deviation, calculated from temperature distribution on the wall inner surface obtained with the conjugate model with the realistic heat flux heating as boundary conditions, the flow is simulated with the 3-D isothermal wall model. As one expected, the overall flow structure predicted by the 3-D isothermal wall model, shown in Fig. 9a, is qualitatively the same as those by the conjugate model (Fig. 6a). In the upper chamber the upward going flow is at the right side (the side with positive temperature deviation) and the downward going flow is at the left side where temperature deviation is negative. The flow has a low velocity magnitude at the top (from $Z/D = 4$ to 5) and at the baffle region (from $Z/D = 0$ to 1) because the flow streams change directions. The center part of the upper chamber, from $Z/D = 1$ to 4, has two vertical flow streams. A similar flow pattern is established in the lower chamber.

The temperature field in the fluid, shown in Fig. 9b, is also qualitatively the same as the conjugate model simulation. Due to the one-cell flow pattern, one can see that the temperature distribution is deformed and is higher at the right half in the upper chamber because the upward flow at the right half carries the high temperature fluid exchanged from the lower chamber through the baffle opening. Comparatively the left half in the upper chamber has a lower temperature.

Flow and temperature simulated by the 2-D isothermal wall model, which does not consider the circumferential temperature/heat-flux deviation, are axially symmetric as shown in Fig. 9c and d respectively. In the upper chamber the upward flow, which carries the high temperature fluid exchanged from the lower chamber, is around the vertical centerline (Z-axis). Flow turns into downward at the top of the upper chamber and flows

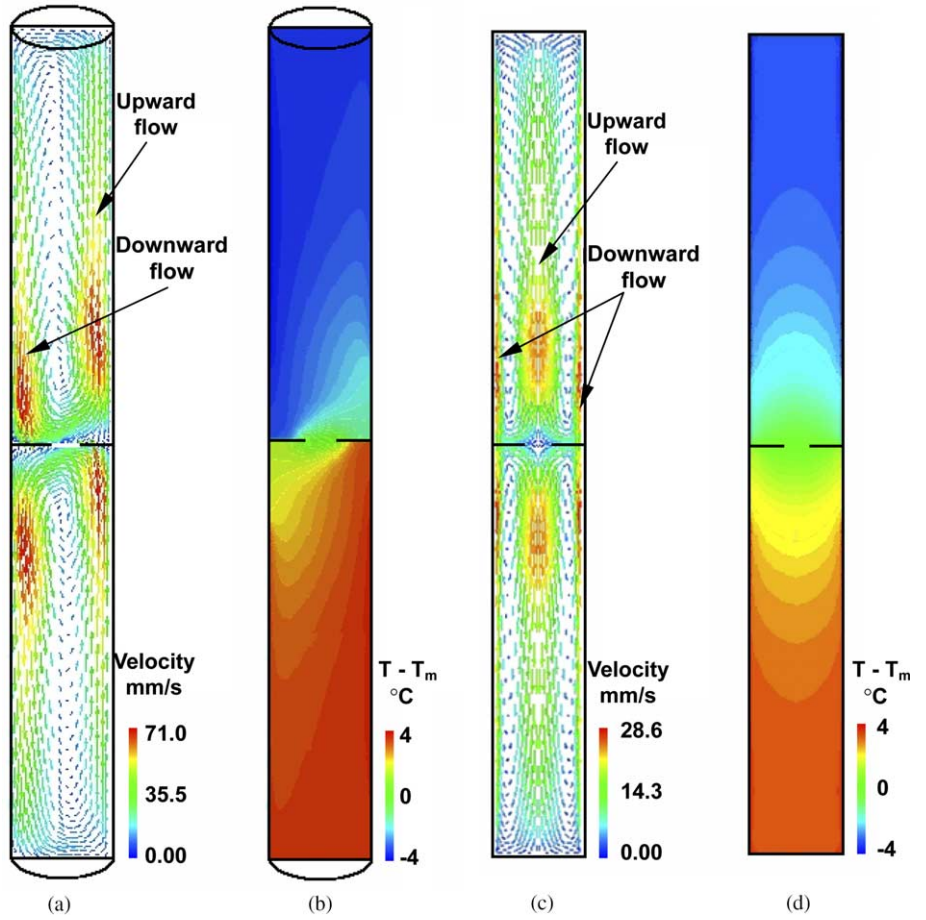

Fig. 9. Velocity and temperature profiles obtained with the isothermal wall models, flow (a) and temperature (b) given by the 3-D isothermal wall model and flow (c) and temperature (d) given by the 2-D isothermal wall model.

downward along the wall until reaches the baffle. Accordingly temperature is higher around the vertical centerline than near the wall.

4.3. Quantitative comparison of the modeling results

With the above description of the modeling results on flow structure and temperature distribution, one can see that results from the 2-D model simulation, which are axially symmetric, are qualitatively different from the flows resulted from the other two models. The flow from the conjugate model and that from the 3-D isothermal wall model are qualitatively the same while quantitatively different, including differences in temperature and flow velocity magnitude.

Fig. 10 shows the vertical velocity at various height locations in the upper chamber obtained with the conjugate model and the two isothermal wall models. One can see that compared to the conjugate model prediction the 3-D isothermal wall model over predicts the velocity magnitude in the upper chamber even though the overall flow patterns are qualitatively the same. The over prediction is caused by the temperature and the temperature deviation set on the boundary. In the conjugate model predictions, the interface temperature and the centerline temperature decrease from the baffle plane to the top (see Figs. 7 and 12). In the 3-D isothermal-wall model, the boundary temperature is set uniform vertically (dashed line in Fig. 7). Even though the temperature and temperature deviation used in the 3-D isothermal-wall model are the averaged ones of the conjugate model, the average temperature difference between the bulk fluid temperature and the wall surface temperature becomes higher in the 3-D isothermal-wall model than in the conjugate model. Higher temperature difference drives a stronger flow. Flow simulated by the 2-D isothermal wall model without considering the asymmetric factors, is axially symmetric and has a much lower velocity magnitude compared to the other two model results.

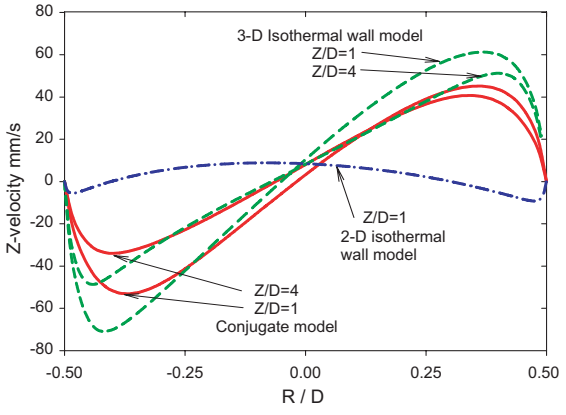

Fig. 10. Comparison of the distribution of the vertical velocities for the three models.

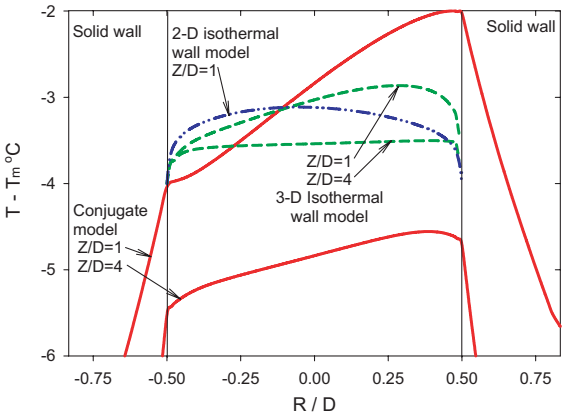

Fig. 11. Comparison of the distribution of the temperature for the three models.

Fig. 11 shows the horizontal temperature distribution in the symmetry plane at various heights in the upper chamber. With the conjugate model, temperature in the horizontal direction is higher at the side with positive heat flux deviation and upward flow and lower at the side with negative heart flux deviation and downward flow. The horizontal temperature difference across the autoclave varies in the vertical direction. Temperature is not uniform on the wall inner surface in both vertical and circumferential directions (see also Fig. 7). With the isothermal wall model, temperatures on the boundaries are constant in the vertical direction for both chambers. By comparing the solid line (from conjugate model) and the dashed line (from 3-D isothermal wall model) one can see that isothermal wall model over predicted the temperature uniformity in the horizontal direction. Prediction with the 2-D isothermal model is also plotted as the dash-dot line in Fig. 11. Since the flow, predicted by the 2-D isothermal wall model, is axisymmetric, the temperature distribution is also axisymmetric and much more uniform compared to the other model simulation results. The conjugate model gives a flow with large horizontal temperature gradient in the fluid while the isothermal models give relatively uniform temperature with large temperature gradient only in the near sidewall region.

Temperatures along the vertical centerline ($R = 0$), by the three models, are given in Fig. 12. The solid line is by the conjugate model while the dashed and dash-dot lines are from the 3-D and 2-D isothermal wall models respectively. Centerline temperatures qualitatively agree with each other. Temperature drop, between the lower chamber and the upper chamber, is mainly at the baffle region. However, centerline temperature obtained with

the conjugate model is not as uniform as those resulted from the isothermal wall models in both chambers. The difference is caused by the constant boundary temperature assumption in the isothermal wall models. The 2-D isothermal wall model gives a more uniform temperature that is more close to the boundary temperature.

Based on the above comparisons one can see that to simulate flow and heat transfer accurately for the current industry autoclaves with uniform heat flux heating on the wall outside surface, the conjugate model should be used. However isothermal wall models can still be used in future study, such as investigation on various baffle designs, because of the following reasons. First, isothermal wall model requires much smaller computing power compared to the conjugate model. Secondly, the isothermal wall model results represent future growth environments and current autoclave design can be improved. A distributed heating, instead of the currently used uniform heat flux heating, can be employed to achieve the constant temperature on the wall/solution interface.

4.4. Remarks on growth environments

Horizontal velocity distribution is important to crystal growers since large velocity gradients cause defects and non-uniform growth. With Fig. 10, one can see that large velocity gradient exist in the near sidewall region no mater the flow is axially symmetric or asymmetric. In the region along the vertical centerline horizontal velocity magnitude variation is comparatively smaller. Due to this fact, crystal growers should mount more seed crystals around the vertical centerline.

Temperature gradient is another important issue for crystal growers since the growth rates are different at different temperatures. In the flow as simulated by the conjugate model crystals grow faster in the upper part in the upper chamber while growth is slower in the near baffle region due to the vertical temperature distribution as shown in Fig. 12. On the other hand, in the flows as simulated by the isothermal wall models, especially the axially symmetric flow, the growth of the crystals in the upper chamber will be much more uniform. Growth in the flow as simulated by the isothermal models, especially the axially symmetric flow, will be more uniform horizontally than in the flow resulted by the conjugate model.

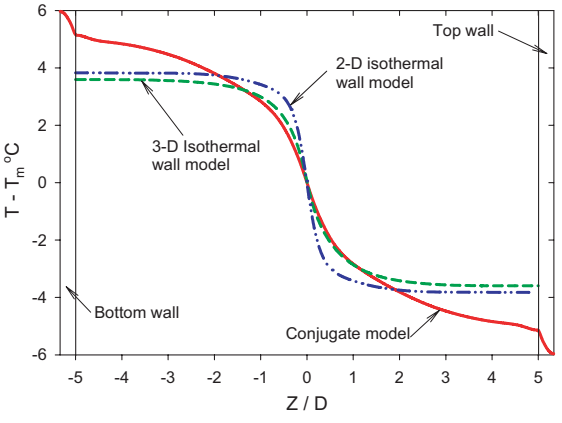

Fig. 12. Centerline temperatures for the three models.

The flow and temperature by the conjugate model (Fig. 6) are more close to the actual growth environments in current industry autoclaves because of the realistic boundary conditions used. However, the uniform temperatures simulated by the isothermal wall models represent growth environments better than those in the current industry production. The flow and temperature given by the 2-D isothermal model, uniform temperature and low flow velocity in the upper chamber, is an ideal crystal growth environment.

Because the boundary conditions, used in the 2-D isothermal wall model, are ideal ones without temperature variation in both vertical and circumferential directions, only autoclaves in very carefully controlled environments can have the axially symmetric pattern [6]. In turn, the cost of the grown crystals will be significantly increased. In current industry production, temperature deviations of small magnitude, while still large enough to change the flow from axially symmetric into axially asymmetric one-cell pattern, exist for most autoclaves.

According to Klipov et al. and the current industry growth experience [4], the direction of the flow surrounding a growing crystal has a significant effect on the growth uniformity. It was observed, for example, that a crystal in the upward flow grows into a wedge shape, thicker at its bottom and thinner at its top while in a downward flow the crystals grow into a wedge shape with thinner bottom and thicker top. With a flow structure as shown in Fig. 6, crystals in the upward and downward flows will grow into different wedge shapes. On the other hand, our previous results show that the flow direction agrees with the superimposed temperature deviation, upward flow in the side with positive temperature deviation [9]. It has also been shown in this paper that the side with positive heat flux wall outer surface has a positive temperature deviation on the wall inner surface. In other words, the one-cell flow direction can be modified by the added heat flux deviation. In order to achieve a more uniform growth, a periodically changing heat flux deviation can be superimposed on the upper chamber wall. The direction of the one-cell flow will follow the heat flux deviation and change accordingly. Seeds in the upward flow in one period will be in the downward flow in the following period. With several flow direction switches during one growth run, the

final grown crystals will have equally thick bottom and top.

5. Conclusions

A conjugate model, with realistic thermal boundary conditions, is set-up to simulate the flow in an industry autoclave for hydrothermal crystal growth. The obtained results show that the flow in an autoclave is axially asymmetric, with one flow cell in each chamber. Temperature isotherms are deformed with the higher temperature in the upward flow and lower temperature in the downward flow in the upper chamber. Flow and temperature in the lower chamber have the patterns anti-symmetric to those in the upper chamber. Temperature on the wall/solution interface is presented. Circumferential temperature deviation on the wall solution interface is large enough to establish the one-cell flow pattern. Quantitative data on both average temperature and temperature deviation are obtained and used in the isothermal wall models. Comparisons of the results from the three models show that 3-D isothermal wall models predicted more uniform temperature. The 2-D isothermal wall model gives an axially symmetric temperature and flow with very low flow strength. Assumptions on the temperature at the wall/solution interface, used in the isothermal wall models, are questionable. By comparing the growth environments obtained by the three models, it seems that the axially symmetric flow is ideal for crystal growth but it is very difficult to achieve. The environment simulated by the 3-D isothermal model is better than that in the current industry. Future autoclave design and flow control should target a uniform temperature on the wall inner surface. It is also proposed that uniform growth can be achieved by periodically switching the direction of the asymmetric flow by changing the superimposed heat flux deviation on the wall outside surface.

Acknowledgements

Founding for this research has been provided by National Science Foundation Combined Research and Curriculum Development (CRCD) Program under Grant Number EEC-9980325. The authors would also like to express sincere thanks to Sawyer Research Products Inc. for the support.

References

[1] L.E. Halliburton, J.J. Martin, D.R. Koehler, Properties of piezoelectric materials, in: E. Gerber, A. Ballato (Eds.), Precision Frequency Control, vol. 1, Academic Press, Inc., 1985, pp. 1–45.
[2] R.A. Laudise, The Growth of Single Crystals, Prentice-Hall, Inc., Englewood Cliffs, NJ, 1970.
[3] K. Byrappa, Hydrothermal growth of crystals, in: D.T.J. Hurle (Ed.), Handbook of Crystal Growth, Elsevier Science B.V., North-Holland, 1994, pp. 465–562.
[4] V.A. Klipov, N.N. Shmakov, Influence of convective flow on the growth of synthetic quartz crystals, in: Proceedings of the Forty Fifth Annual Symposium on Frequency Control, IEEE, 1991, pp. 29–36.
[5] V.A. Kuznetsov, A.N. Lobachev, Hydrothermal method for the growth of crystals, Sov. Phys.—Crystallogr. 17 (4) (1973) 775–804.
[6] B. Roux, O. Louchart, O. Terhmina, Hydrodynamic aspect of hydrothermal synthesis of quartz bulk flow regimes, J. de Physique IV (Colloque C2, supplement au J. de Physique III) 4 (1994) C2-3–C2-11.
[7] Q.S. Chen, V. Prasad, A. Chatterjee, J. Larkin, A porous media-based transport model for hydrothermal growth, J. Cryst. Growth 198/199 (Part 1) (1999) 710–715.
[8] Q.S. Chen, V. Prasad, A. Chatterjee, J. Larkin, Modeling of fluid flow and heat transfer in a hydrothermal crystal growth system: use of fluid-superposed porous layer theory, J. Heat Transfer—Trans. ASME 121 (4) (1999) 1049–1058.
[9] H. Li, E.A. Evans, G.-X. Wang, Flow of solution in hydrothermal autoclaves with various aspect ratios, J. Cryst. Growth 256 (1–2) (2003) 146–155.
[10] H. Li, G.-X. Wang, E.A. Evans, Three-dimensional flow of solution in an autoclave subjected to non-uniform heating—effects of a baffle on flow and temperature separations, J. Cryst. Growth 271 (1–2) (2004) 257–267.
[11] D.C. Wilcox, Turbulence Modeling for CFD, DCW Industries Inc., 1994.
[12] AEA Technology, Physical models and fluid properties, in: Solver manual CFX-4.2, 1997, pp. 55–85.
[13] F. Ampofo, T.G. Karayiannis, Experimental benchmark data for turbulent natural convection in air filled square cavity, Int. J. Heat Mass Transfer 46 (19) (2003) 3551–3572.